AIP Journal of Applied Physics

Saddle-like deformation in a dielectric elastomer actuator embedded with liquid-phase gallium-indium electrodes

J. Wissman, L. Finkenauer, L. Deseri, and C. Majidi

Citation: Journal of Applied Physics **116**, 144905 (2014); doi: 10.1063/1.4897551
View online: http://dx.doi.org/10.1063/1.4897551
View Table of Contents: http://scitation.aip.org/content/aip/journal/jap/116/14?ver=pdfcov
Published by the AIP Publishing

JOURNAL OF APPLIED PHYSICS **116**, 144905 (2014)

Saddle-like deformation in a dielectric elastomer actuator embedded with liquid-phase gallium-indium electrodes

J. Wissman,[1,a),b)] L. Finkenauer,[1,2,a)] L. Deseri,[3,4,5] and C. Majidi[1,6]
[1]*Department of Mechanical Engineering, Carnegie Mellon University, Pittsburgh, Pennsylvania 15213, USA*
[2]*Department of Materials Science and Engineering, Carnegie Mellon University, Pittsburgh, Pennsylvania 15213, USA*
[3]*DICAM, Department of Mechanical, Civil and Environmental Engineering, University of Trento, via Mesiano 77 38123 Trento, Italy*
[4]*TMHRI-Department of Nanomedicine, The Methodist Hospital Research Institute, 6565 Fannin St., MS B-490 Houston, Texas 77030, USA*
[5]*Mechanics, Materials and Computing Center, CEE & ME-CIT, Carnegie Mellon University, Pittsburgh, Pennsylvania 15213, USA*
[6]*Robotics Institute and Department of Civil and Environmental Engineering, Carnegie Mellon University, Pittsburgh, Pennsylvania 15213, USA*

(Received 28 July 2014; accepted 29 September 2014; published online 14 October 2014)

We introduce a dielectric elastomer actuator (DEA) composed of liquid-phase Gallium-Indium (GaIn) alloy electrodes embedded between layers of poly(dimethylsiloxane) (PDMS) and examine its mechanics using a specialized elastic shell theory. Residual stresses in the dielectric and sealing layers of PDMS cause the DEA to deform into a saddle-like geometry (Gaussian curvature $\mathcal{K} < 0$). Applying voltage Φ to the liquid metal electrodes induces electrostatic pressure (Maxwell stress) on the dielectric and relieves some of the residual stress. This reduces the longitudinal bending curvature and corresponding angle of deflection ϑ. Treating the elastomer as an incompressible, isotropic, NeoHookean solid, we develop a theory based on the principle of minimum potential energy to predict the principal curvatures as a function of Φ. Based on this theory, we predict a dependency of ϑ on Φ that is in strong agreement with experimental measurements performed on a GaIn-PDMS composite. By accurately modeling electromechanical coupling in a soft-matter DEA, this theory can inform improvements in design and fabrication. © *2014 AIP Publishing LLC*.
[http://dx.doi.org/10.1063/1.4897551]

I. INTRODUCTION

Dielectric elastomer actuators (DEAs) represent a promising alternative to conventional actuator technologies for powering soft bio-inspired robots, assistive wearable technologies, and other systems that depend on mechanical "impedance matching" with soft biological tissue. In contrast to electrical motors and hydraulics, DEAs can be made entirely out of soft elastic materials and fluids and remain functional under extreme bending and stretching. Moreover, they operate with very little electrical power and can exhibit as much as 90% efficiency of electrical energy input to mechanical work output. While there have been significant improvements since early studies in the late 1990s, progress in DEA performance and robotics implementation continues to depend on advancements in materials selection, design, and predictive theoretical modeling of the underlying elasticity and electromechanical coupling.

Here, we introduce a DEA composed of liquid-phase Gallium-Indium (GaIn) alloy electrodes embedded between layers of poly(dimethylsiloxane) (PDMS).[1] In contrast to existing DEA designs, which contain inextensible (but flexible) frames,[2] springs,[3] or solid electrodes,[4] the mechanics of the GaIn-embedded composite is governed entirely by the elasticity of the surrounding PDMS elastomer. Moreover, we observe that the composite forms a saddle-shape and exhibits a relationship between longitudinal bending curvature and voltage that cannot be predicted with a classical bending beam model (see, e.g., Sect. 4.2.2 of Ref. 5). Instead, we use a kinematically parameterized shell theory and use the Rayleigh-Ritz technique for minimum potential energy to estimate the shape of the DEA at static equilibrium. We find that the theoretical predictions are in strong agreement with experimental measurements (without the aid of data fitting) so long as we allow for negative Gaussian curvature ($\mathcal{K} < 0$). In addition to furnishing an accurate prediction for the GaIn-PDMS composite, we are confident that this modeling approach can be extended to other DEA materials and designs.

DEAs are composed of a soft insulating elastomer film coated with conductive fluid or rubber electrodes. Applying a potential difference Φ to the electrodes induces an electrostatic pressure (Maxwell stress) on the embedded dielectric layer. As with a capacitor, nearly no current is drawn by the DEA, and thus very little power is expended. The dielectric is frequently created with a soft elastomer, such as acrylic-based VHB tape (3M^{TM}) or PDMS. DEA designs include diaphragms,[6] bimorphs,[7,8] rolls,[7,9] and reinforced planar stacks[10,11] and exhibit a variety of motions, load capacities, and electromechanical coupling.

[a)]J. Wissman and L. Finkenauer contributed equally to this work.
[b)]Author to whom correspondence should be addressed. Electronic mail: jwissman@andrew.cmu.edu

A central challenge in DEA development is the selection of "stretchable" electrodes that do not constrain the elastic deformation of the embedded dielectric layer.[12] Typically, the surfaces of the dielectric are coated with metallic particles,[13] graphite powder,[7] carbon fibers,[7] carbon black,[11] or carbon grease.[9,14] Alternatively, DEAs may comprise conductive electrode materials such as electrolytic elastomers (hydrogels)[15] or electrodes made conductive by direct filling with conductive particles[8] or through low-energy ion implantation.[6] Fabrication methods include spraying, stamping, printing, laser-cutting, and spin-coating, or creating thin-film metal trace electrodes of copper, silver or gold using electroplating, sputtering, evaporation and patterning with photolithography.[12] While carbon based electrodes are relatively cheap and easy to fabricate, they have inherently high electrical resistivity and are often grainy and inconsistent at thinner layer thicknesses. In contrast, thin film metallic electrodes are highly conductive and easily patterned, but add to the stiffness of the DEA and require clever fabrication to undergo stretching (e.g., pre-buckling and wavy electronics[16]).

Liquid-phase GaIn alloys represent a promising alternative to existing carbon based and solid electrode materials.[17,18] Like carbon grease, it does not interfere with the mechanics of the surrounding elastomer and remains conductive during stretching. However, it exhibits 3–6 orders of magnitude less electrical resistance, with a conductivity only 1/20th that of conventional copper wiring. Liquid GaIn has already been used for soft and stretchable wiring,[19] sensors,[20] and electronics.[21] Microfluidic channels of liquid alloy are typically produced with replica molding and needle injection using techniques adapted from "soft" lithography and microfluidics.[22] However, DEAs require a thin film coating of liquid alloy that cannot be produced using needle injection. Instead, they must be produced with techniques like laser machining,[23] masked deposition,[24] or stencil lithography.[25,26]

The dielectric in a DEA is typically modeled as an incompressible elastic solid subject to a Maxwell stress $\sigma_M = \epsilon_r \epsilon_0 \mathbf{E}^2$, where ϵ_0 is the permittivity of free space, ϵ_r is a dielectric constant, and $\mathbf{E}$ is the electric field strength.[7,27–29] Recently, researchers have examined dynamics,[30] resonance,[31,32] and failure of thin film dielectrics[33,34] and the effect of viscoelasticity on electric instabilities and fracture.[35] In most cases, the elastomer in a DEA undergoes elastic strains and bending curvatures that are beyond the scope of linearized theories for elastic plates and shells. Instead, we must use a non-classical shell theory that treats the elastomer as an incompressible hyperelastic solid. For moderate stretch, we can model the PDMS layers with a NeoHookean constitutive law that only requires a single coefficient of elasticity.[36] For larger strains, we must use a Mooney-Rivlin,[37,38] Ogden,[39] or any other model that allows for nonlinear elasticity with two or more coefficients.

II. EXPERIMENTAL METHODS

The GaIn-PDMS composite is produced using the steps presented in Fig. 1.[1] The PDMS dielectric layer (SYLGARD® 184; Dow Corning) is first applied on a flat substrate using a 5 μm resolution thin film applicator (ZUA 2000 Universal Applicator, Zehntner GmbH). After curing on a hot plate, eutectic GaIn (EGaIn, $\geq$99.99%; Sigma-Aldrich) electrodes are manually deposited using an elastomeric blotter and laser-patterned (VLS3.50, Universal Laser Systems) stencil.[26] After deposition, the mask is carefully removed and an encapsulating layer of PDMS is applied over the exposed liquid electrodes. Before this sealing step, a thin strip of adhesive-backed conductive paper (3M™ Fabric Tape CN-3490) is placed in contact with each patterned liquid metal electrode for eventual interfacing with external electronics. Following another cure on the hot plate, the composite PDMS-EGaIn-PDMS film is carefully peeled and flipped in order to expose the other side of the dielectric layer, and a second set of electrodes is applied in the same way. The pre-strain required for inducing curvature is achieved by manually stretching the DEA by 6% and allowing it to naturally adhere to a substrate. Lastly, a thicker layer of PDMS elastomer is applied over the stretched DEA. The sealing layer, dielectric layer (separating the embedded electrodes), and substrate layer have thicknesses of $H_1 = 163$ μm, $H_2 = 85$ μm, and $H_3 = 490$ μm, respectively.

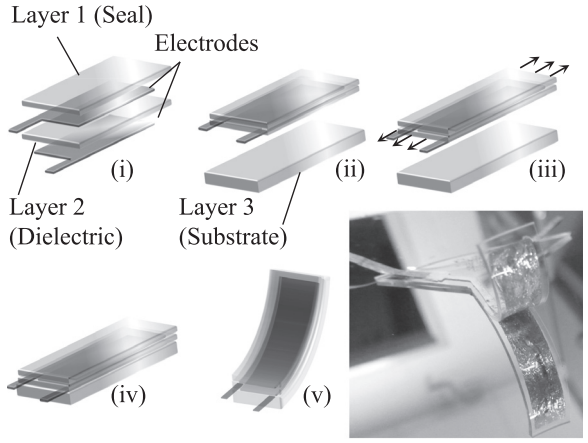

FIG. 1. Illustration of DEA layer components during fabrication showing (i) encapsulated electrodes and compliant electrode layers, (ii)–(iv) straining of DEA composite and bonding to an initially unstrained substrate polymer layer, and (v) curved configuration of released actuator with picture of actual device.

The resulting curved DEA is connected to a 10 kV high voltage transformer (Q101-5, EMCO High Voltage Corporation) via conductive paper leads and placed on an isolated substrate. A high voltage probe (PR 28A HV DMM Probe, B&K Precision) attenuates by 1000× the voltage across the actuator for real-time recording via an Arduino UNO R3 microcontroller with a custom MATLAB GUI interface. Recorded footage of the device actuating as the voltage is slowly ($\approx$0.02 Hz) ramped up and down from 0.0–5.0 kV is evaluated using a video analysis and modeling software (Tracker; https://www.cabrillo.edu/~dbrown/tracker/). We extract data on deformation (bending) as a function of time by monitoring the changing beam tip deflection with the aid of the automated object tracking tool. The voltage can then be interpolated and correlated with the Tracker output based on time stamps for a complete description of actuation in response to voltage.

III. THEORY

In its *natural* (i.e., isolated, stress-free) state, each PDMS layer of the DEA is a right rectangular prism with length L_i, width W_i, and thickness H_i as shown in Fig. 3. As illustrated in Fig. 1, the index $i \in \{1,2,3\}$ identifies the layer (*layer 1*—sealing layer; *layer 2*—dielectric layer coated with electrodes on the top and bottom surfaces; *layer 3*—thick elastomer substrate). In order to induce residual bending curvature in the DEA, layers 1 and 2 have dimensions $L_1 = L_2 < L_3$ and $W_1 = W_2 \geq W_3$. To assemble the DEA, layers 1 and 2 are bonded together and then stretched so that they share the same length and width as layer 3. When the third layer is bonded, the composite deforms in order to relieve the residual strains in the pre-stretched layers. In general, this deformation involves changes in the width, length, and bending curvature(s) of the composite. Moreover, the shape of the DEA at static equilibrium changes when electrical voltage Φ is applied to the electrodes. Fig. 2 shows the direction of beam deflection with applied voltage Φ, which results in a changing ϑ (defined as half of the arc angle $\bar{\theta}$ shown in Fig. 3). We observe that in addition to bending about its intermediate (width-wise) axis, the GaIn-PDMS composite also bends in the opposite direction about its major (length-wise) axis to form a saddle-like shape. Pure bending (zero Gaussian curvature, i.e., $\mathcal{K} = 0$ and saddle-like deformation ($\mathcal{K} < 0$) are examined separately in Subsections III A and III B. In both cases, the bending curvature about the intermediate axis decreases as the applied voltage Φ increases.

A. Pure bending

One method for modeling the device is to simplify the kinematics by ignoring saddle formations and assuming a plane strain condition. Under this description, each layer is of equal width W regardless of deformation. The result is pure bending where the DEA curls into a circular arc with an inner radius of ρ and an arc angle of $\bar{\theta}$ (see Fig. 3).

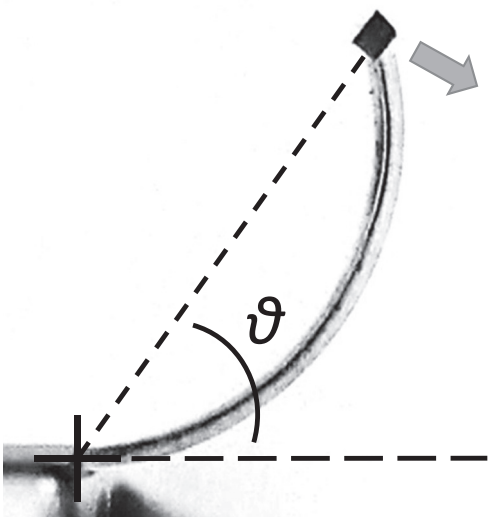

FIG. 2. Side view of soft-matter PDMS-GaIn DEA composite during testing.

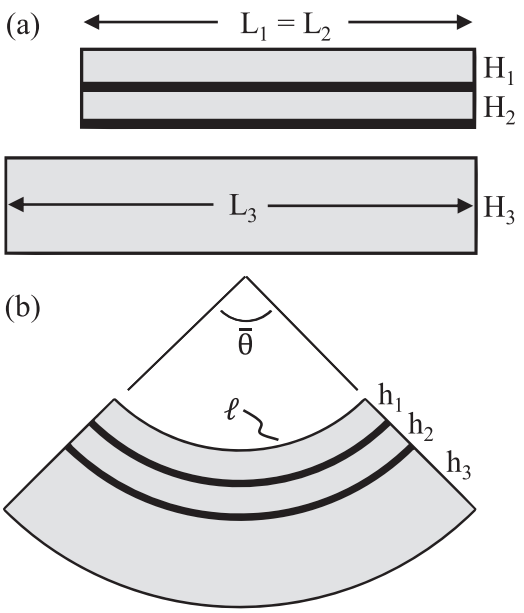

FIG. 3. (a) Actuator cross-section with dimensions before assembly (electrodes marked by black lines shown only for illustrative purposes and are not included in the thickness dimensions). (b) Actuator cross-section after assembly.

Alternatively, the inner radius can be described in terms of curvature κ and length ℓ. Furthermore, the liquid metal electrodes are assumed to be infinitely thin, and a NeoHookean constitutive model is employed for the PDMS elastomer. (NeoHookean is deemed appropriate because strains are less than 10%.) The strain energy density shown below can be determined with the three principal stretches (λ_i) and a material coefficient of elasticity $C_1 = Y/6$, where Y is the Young's modulus for uniaxial loading

$$\psi = C_1(\lambda_1^2 + \lambda_2^2 + \lambda_3^2 - 3). \tag{1}$$

We define λ_θ, λ_n, and λ_z as principal stretches. The symbol λ_θ refers to the stretch along the arc length ($\mathbf{e}_\theta$), λ_n to the width ($\mathbf{e}_n$), and λ_z to the thickness ($\mathbf{e}_z$). Incompressibility dictates that the product of these three stretch values must be equal to 1, and so the plane strain condition implies $\lambda_n = 1$ and $\lambda_z(z) = 1/\lambda_\theta$. The stretch $\lambda_\theta(z)$ can be quantified as $\ell(1+\kappa z)/L_i$, where z the position of material radially from the inner surface. The elastic strain energy Ω can then be determined by plugging the stretch values into the NeoHookean energy density equation (1) and integrating over the unstrained, material volume: $\Omega = \Omega_1 + \Omega_2 + \Omega_3$,

$$\psi_i = C_1\left\{\left(\frac{\ell}{L_i}(1+\kappa z)\right)^2 + \left(\frac{\ell}{L_i}(1+\kappa z)\right)^{-2} - 2\right\}, \tag{2}$$

$$\Omega_1 = \int_0^{H_1} \psi_1 W L_1\, dz, \tag{3}$$

$$\Omega_2 = \int_{H_1}^{H_1+H_2} \psi_2 W L_2\, dz, \tag{4}$$

$$\Omega_3 = \int_{H_1+H_2}^{H_1+H_2+H_3} \psi_3 W L_3\, dz. \tag{5}$$

Equivalently, the stretch $\lambda_\theta(z)$ can be quantified as $\bar{\theta}(\rho+z)/L_i$. As before, $\lambda_n = 1$ and $\lambda_z(z) = 1/\lambda_\theta$. Because the elastomer is incompressible, the elastic strain energy can be calculated by integrating over the dimensions in the final configuration, where h_i refers to the deformed thickness of each layer which can be determined based on the stretch definitions and the actuator geometry

$$\psi_i = C_1\left\{\left(\frac{\bar{\theta}(\rho+z)}{L_i}\right)^2 + \left(\frac{\bar{\theta}(\rho+z)}{L_i}\right)^{-2} - 2\right\}, \quad (6)$$

$$\Omega_1 = \int_0^{h_1} \psi_1(\rho+z)W\bar{\theta}\,dz, \quad (7)$$

$$\Omega_2 = \int_{h_1}^{h_1+h_2} \psi_2(\rho+z)W\bar{\theta}\,dz, \quad (8)$$

$$\Omega_3 = \int_{h_1+h_2}^{h_1+h_2+h_3} \psi_3(\rho+z)W\bar{\theta}\,dz. \quad (9)$$

For the electrostatic energy, the electric field as a function of ρ can be determined using Maxwell's equations. To begin, we assume no charge builds within the elastomer, so the divergence of the electric field (gradient of the potential φ) is known to be zero between and outside the electrodes. The result is the following differential equation with respect to z: $\varphi_{,zz} + (1/(\rho+z))\varphi_{,z} = 0$. Furthermore, we can describe the potential at the electrodes as $\Phi/2$ and $-\Phi/2$, where Φ is the applied voltage drop. The change in potential with respect to z is assumed to be negligible outside of the electrodes. This boundary value problem yields the following solution for the electric field:

$$\mathbf{E} = \frac{\Phi}{(\rho+z)\ln\left[(\rho+h_1+h_2)/(\rho+h_1)\right]}. \quad (10)$$

The electrostatic contribution U_ϕ to the total potential energy is

$$U_\phi = -\int_{h_1}^{h_1+h_2} \frac{1}{2}\epsilon_r\epsilon_0\mathbf{E}^2(\rho+z)\bar{\theta}(W-2b)dz\,, \quad (11)$$

which corresponds to an "electrical enthalpy." Here, $\epsilon_0 = 8.85\times10^{-12}$ F/m is the vacuum permittivity and ϵ_r again is the relative electrical permittivity (i.e., dielectric constant). Also, the dimension b (0.75 μm) represents the width of the PDMS border in the plane of the liquid GaIn electrodes. Electrostatic energy can also be approximated by assuming that the electrodes form a parallel plate capacitor. The width of this capacitor is W_e, the electrode separation h_2, and the length is approximated as $\ell_D = L_2\lambda_\theta$ where λ_θ is evaluated at $z = h_1 + h_2/2$. The capacitance C is then determined and used to calculate U_ϕ

$$C \approx \frac{\epsilon_r\epsilon_0 W_e\ell_D}{h_2}, \quad (12)$$

$$U_\phi = -\frac{1}{2}C\Phi^2 = -\frac{\epsilon_r\epsilon_0 W_e\ell_D\Phi^2}{2h_2}. \quad (13)$$

Lastly, at static equilibrium, the combined energy $\Pi = \Omega + U_\phi$ must be minimized with respect to the free kinematic parameters ρ and $\bar{\theta}$. Note that $\{\rho, \bar{\theta}\}$ and $\{\ell, \kappa\}$ are geometrically related and can be interchanged. This can be performed numerically with a multivariable optimization or by finding the solution to the two linearly independent equations $\partial\Pi/\partial\rho = 0$ and $\partial\Pi/\partial\bar{\theta} = 0$. For the work presented here, the combination of current volume strain energy and Maxwell's solution and the combination of material volume strain energy and capacitor approximation result in nearly equivalent results.

B. Saddle-like deformation

In practice, we observe that the DEA deforms into a saddle-like shape with negative Gaussian curvature $\mathcal{K} = -\kappa_\theta\kappa_\phi$, where κ_θ and κ_ϕ are the principal curvatures along the length ($\mathbf{e}_\theta$) and width ($\mathbf{e}_\phi$), respectively. In order to examine the dependency of $\{\kappa_\theta, \kappa_\phi\}$ on Φ, we consider three representations (placements) of the elastic layers. In the *natural* placement, each layer is isolated and has dimensions $\{L_i, W_i, H_i\}$. In the *reference* placement the pre-stretched layers (1 and 2) are bonded to the thick substrate (layer 3) and the composite relaxes into a rectangular prism of length ℓ and width w. Here, each point has Euclidean coordinates $\{X, Y, Z\}$ where the tangent bases $\{\mathbf{e}_X, \mathbf{e}_Y, \mathbf{e}_Z\}$ are oriented along the composite length, width, and thickness, respectively. Lastly, in the *current* placement, the composite deforms such that the top of layer 1 (sealing layer) forms a *saddle surface* $\mathcal{S}_1$ with dimensions $\{\ell, w\}$ and principal curvatures $\{\kappa_\theta, \kappa_\phi\}$ as defined below. Here, each point has "inverted" spherical coordinates $\{\theta, \phi, z\}$ and the coordinate lines have tangent (covariant) vectors $\{\mathbf{e}_\theta, \mathbf{e}_\phi, \mathbf{e}_z\}$. The coordinates $\{\theta, \phi, z\}$ along with the arcangles $\{\bar{\theta}, \bar{\phi}\}$ and radii of curvature $\rho_\theta = \kappa_\theta^{-1}$ and $\rho_\phi = \kappa_\phi^{-1}$ for the $\mathcal{S}_1$ centerlines are defined in Fig. 4.

Assuming that points in the $\mathbf{e}_X - \mathbf{e}_Z$ and $\mathbf{e}_Y - \mathbf{e}_Z$ planes of the reference placement remain plane, the $\mathbf{e}_\theta - \mathbf{e}_\phi$ surfaces form saddles $\mathcal{S}$. For each z, $\mathcal{S}$ has centerlines with

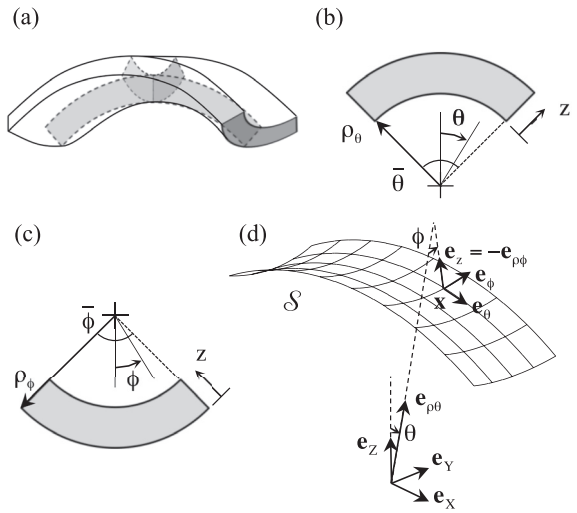

FIG. 4. (a) DEA composite deforms to form a saddle-like geometry. (b) Deformation in the $\mathbf{e}_\theta - \mathbf{e}_z$ plane shows bending with radius $\rho_\theta = \kappa_\theta^{-1}$ in the longitudinal direction. (c) Deformation in the $\mathbf{e}_\phi - \mathbf{e}_z$ plane shows bending with radius $\rho_\phi = \kappa_\phi^{-1}$ in the width-wise direction. (d) Position of a point $\mathbf{x}$ within a saddle surface $\mathcal{S}$.

arcangles $\bar{\theta} = \kappa_\theta \ell$ and $\bar{\phi} = \kappa_\phi w$ and radii of curvature $\rho_\theta + z$ and $\rho_\phi - z$. The coordinate lines along the $\mathbf{e}_\theta$ and $\mathbf{e}_\phi$ directions have total lengths of $\ell_\theta = \{(\rho_\theta + z) + (1 - \cos\phi)(\rho_\phi - z)\}\bar{\theta}$ and $w_\phi = (\rho_\phi - z)\bar{\phi}$, respectively. Referring to Fig. 4, a point in $\mathcal{S}$ has a position

$$\mathbf{x} = \mathbf{x}(\theta, \phi, z) = (\rho_\theta + \rho_\phi)\mathbf{e}_{\rho\theta}(\theta) + (\rho_\phi - z)\mathbf{e}_{\rho\phi}(\theta, \phi)\,, \tag{14}$$

where $\mathbf{e}_{\rho\theta} = \sin\theta \mathbf{e}_X + \cos\theta \mathbf{e}_Z$ and $\mathbf{e}_{\rho\phi} = \sin\phi \mathbf{e}_Y - \cos\phi \mathbf{e}_{\rho\theta}$.

For each z, the saddle surface $\mathcal{S}$ has an area of

$$a(z) = \left\{[\rho_\theta + \rho_\phi]\bar{\phi} - 2(\rho_\phi - z)\sin\left(\frac{\bar{\phi}}{2}\right)\right\}\bar{\theta}(\rho_\phi - z)\,. \tag{15}$$

Each layer of the composite is assumed to be incompressible and so the final thicknesses h_i can be estimated by dividing the initial volume by the final area of its top surface: $h_i \approx W_i L_i H_i / a_i$, where $a_1 = a(0)$, $a_2 = a(h_1)$, and $a_3 = a(h_1 + h_2)$. The final layer thicknesses h_i are only approximations because they are calculated using the area of the top surface rather than mid-plane of each layer. Moreover, the exact layer thickness will be non-uniform since the principal stretch λ_θ in the $\mathbf{e}_\theta$ direction increases with $|\phi|$. Nonetheless, the above approximations are used since it allows the thickness to be estimated *explicitly* by calculating a_1, h_1, a_2,..., h_3 in sequence.

Each layer is treated as a *hyperelastic* solid with principal stretches $\{\lambda_\theta, \lambda_\phi, \lambda_z\}$ in the $\{\mathbf{e}_\theta, \mathbf{e}_\phi, \mathbf{e}_z\}$ directions and a strain energy density $\psi = \psi(\lambda_\theta, \lambda_\phi, \lambda_z)$. The stretches λ_θ and λ_ϕ are calculated by dividing the arclength of each convecting coordinate line by its original length in the natural placement: $\lambda_\theta(\phi, z) = \ell_\theta / L_i$ and $\lambda_\phi(z) = w_\phi / W_i$, where $i = 1$, 2, and 3 for $z \in [0, h_1)$, $[h_1, h_1 + h_2)$, and $[h_1 + h_2, h_1 + h_2 + h_3]$, respectively. Incompressibility implies $\lambda_z = 1/\lambda_\theta\lambda_\phi$ and that the total elastic strain energy $\Omega = \sum_{i=1}^{3} \Omega_i$ can be calculated by integrating ψ in the current placement where now Ω_i are evaluated as follows:

$$\Omega_1 = \int_0^{h_1} \int_{-\bar{\phi}/2}^{\bar{\phi}/2} \psi \ell_\theta (\rho_\phi - z)\, d\phi\, dz, \tag{16}$$

$$\Omega_2 = \int_{h_1}^{h_1+h_2} \int_{-\bar{\phi}/2}^{\bar{\phi}/2} \psi \ell_\theta (\rho_\phi - z)\, d\phi\, dz, \tag{17}$$

$$\Omega_3 = \int_{h_1+h_2}^{h_1+h_2+h_3} \int_{-\bar{\phi}/2}^{\bar{\phi}/2} \psi \ell_\theta (\rho_\phi - z)\, d\phi\, dz\,. \tag{18}$$

For a pre-strain of $<10\%$ in layers 1 and 2, we expect only moderate stretches at static equilibrium. Therefore, we again treat the composite as a NeoHookean solid and let

$$\psi = 2C_1\left(\lambda_\theta^2 + \lambda_\phi^2 + \frac{1}{\lambda_\theta^2\lambda_\phi^2} - 3\right), \tag{19}$$

where $C_1 = Y/6$ is the coefficient of elasticity as before.

When voltage Φ is applied, the DEA has a total potential energy $\Pi = \Omega + U_\phi$, where U_ϕ is the electrical enthalpy. Since the electrodes are surrounded by a border that is $b = 0.75$ mm wide, the final area is approximately χa_2, where $\chi = (W_2 - 2b)(L_2 - 2b)/W_2 L_2$. In the current placement (i.e., saddle-shape configuration), the capacitance between the two electrodes is estimated as $C \approx \chi\epsilon_r\epsilon_0 a_2 / h_2$ and the electrical enthalpy is

$$U_\phi = -\frac{1}{2}C\Phi^2 = -\chi\frac{\epsilon_r\epsilon_0 a_2 \Phi^2}{2h_2}\,. \tag{20}$$

Lastly, the unknown kinematic parameters $\{w, \ell, \kappa_\theta, \kappa_\phi\}$ are determined by minimizing the total potential energy Π. This may be accomplished either by performing a multivariable optimization or finding the solution to the stationary conditions $\partial\Pi/\partial w = \partial\Pi/\partial\ell = \partial\Pi/\partial\kappa_\theta = \partial\Pi/\partial\kappa_\phi = 0$. While both approaches are valid, numerical minimization is more convenient since it eliminates the additional step of calculating the partial derivatives of Π.

IV. RESULTS AND DISCUSSION

Results from the experiments and theory are presented in Fig. 5. The grey dots correspond to experimental measurements collected from a single DEA sample and the dashed-dotted curve are theoretical predictions from the simplified pure bending model. The pure bending theory overestimates the angle of deflection by approximately 9°. Furthermore, it exaggerates the change $\Delta\vartheta$ in arcangle $\vartheta = \bar{\theta}/2$ as a function of applied voltage Φ. This is most likely because the plane strain assumption underestimates the final thickness of the dielectric, causing an overestimate of the electrostatic component of the potential (particularly at higher strains and voltages). The lack of saddling may also play a role in the misrepresentation of $\Delta\vartheta$ since the effective area moment of inertia is underestimated.

The general saddling theory presented yields predictions, represented by the solid curve with circular markers, which are in much stronger agreement with the experimental measurements. These predictions correspond to a uniaxial pre-stretch of layers 1 and 2 during the DEA assembly. As

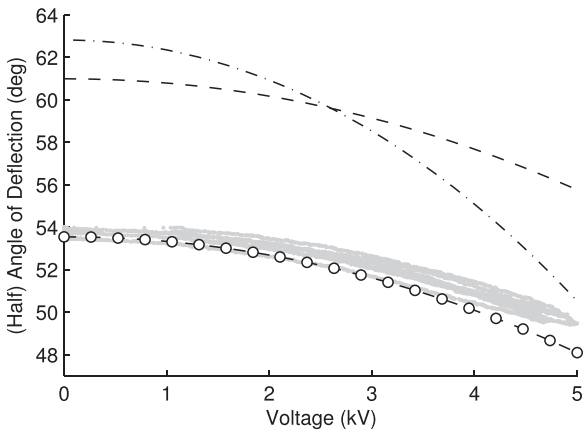

FIG. 5. Comparison of experimental measurements and theoretical predictions for the arcangle $\vartheta = \bar{\theta}/2$ as a function of applied voltage Φ: (gray dots) experimental data collected from repeated measurements on a single DEA sample; (dash-dot) the theoretical prediction based on the simplified pure bending model; (circles) prediction from the generalized theory with "uniaxial" pre-stretch; (dashed) prediction with "plane strain" pre-stretch.

discussed above, the two layers are first bonded together and stretched so that they share the same width and length of layer 3. For pure uniaxial loading, the two layers stretch by an amount $\hat{\lambda}_X = L_3/L_1 = L_3/L_2$ in the $\mathbf{e}_X$ direction and $\hat{\lambda}_Y = \hat{\lambda}_Z = \hat{\lambda}_X^{-1/2}$ in the $\mathbf{e}_Y$ and $\mathbf{e}_Z$ directions. This requires an initial width $W_1 = W_2 = W_3/\hat{\lambda}_Y = W_3\sqrt{L_3/L_1}$. We use the term "uniaxial" since the elastomer is under uniaxial stress during pre-stretch with the condition $\sigma_Y = \sigma_Z = 0$ implying $\hat{\lambda}_Y = \hat{\lambda}_Z$.

The theoretical prediction appears to be in strong agreement with the experimental measurements (without the aid of data fitting). While the resulting observed change in bending curvature is less than has been demonstrated by other unimorph type DEAs,[13] our device both takes into account saddling due to pre-stretch and also displays no obvious degradation of the electrode material throughout testing (though a much more extensive study is necessary to verify this claim). However, the theory suggests that even greater bending can be achieved by imposing a "plane strain" loading condition during pre-stretch. To accomplish this, layers 1 and 2 should be constrained such that $\hat{\lambda}_Y = 1$ during pre-stretch. Theoretical predictions based on this case where $W_1 = W_2 = W_3$ are presented by the dashed curve in Fig. 5. This prediction preserves the dependency of $\Delta\vartheta$ on Φ but increases the absolute angle of deflection by approximately 7°. The greater bending angle is attributed to a dramatic reduction in transverse curvature (see Fig. 6), which allows for almost pure bending deformation. Here, "plane strain" refers to the constraint that strain only in the $\mathbf{e}_X - \mathbf{e}_Z$ plane. However, this could also be interpreted as a "plane stress" assumption where stress is restricted to the $\mathbf{e}_X - \mathbf{e}_Y$ plane (i.e., $\sigma_Z = 0$).

Fig. 6 compares curvatures in the two bending planes of the saddle-shaped DEA. For uniaxial pre-stretch, the bending curvatures in the $\mathbf{e}_\theta - \mathbf{e}_z$ (open circles) and $\mathbf{e}_\phi - \mathbf{e}_z$ (open triangles) planes are approximately $\kappa_\theta \sim 84$–$93\,\mathrm{m}^{-1}$ and $\kappa_\phi \sim 32$–$39\,\mathrm{m}^{-1}$, respectively. This relatively high degree of saddling can be explained by Poisson's effect as the actuator bends. Although the DEA layer is generally in tension while the initially unstrained layer is in compression, the uniaxial pre-stretch results in an approximately constant width with respect to z ($\kappa_\phi \approx 0$) if κ_θ is forced to zero by some external moment. However, as the beam bends, material towards the inner surface experiences more compression and width expansion, causing the saddle formation ($\kappa_\phi > 0$). Unlike an external moment, which lengthens the DEA layer but shortens its width, electrostatic pressure during actuation leads to an increase in both width and length. As a result of the width expansion, actuation induces an increase in κ_ϕ.

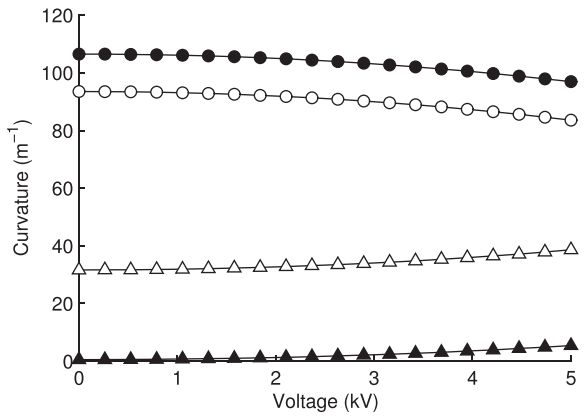

FIG. 6. Comparison of predicted bending curvatures κ_θ and κ_ϕ in the (circles) $\mathbf{e}_\theta - \mathbf{e}_z$ and (triangles) $\mathbf{e}_\phi - \mathbf{e}_z$ planes: (open markers) uniaxial pre-stretch; (filled markers) plane strain pre-stretch.

For plane strain pre-stretch, bending in the $\mathbf{e}_\theta - \mathbf{e}_z$ plane (filled circles) is greater ($\kappa_\theta \sim 97$–$107\,\mathrm{m}^{-1}$), however the curvature in the $\mathbf{e}_\phi - \mathbf{e}_z$ plane (filled triangles) is almost negligible ($\kappa_\phi \sim 0.5$–$5\,\mathrm{m}^{-1}$). Unlike the uniaxial case, one would expect a negative κ_ϕ to form if κ_θ were reduced to zero by an external moment; due to the plane strain, the DEA layer would attempt to contract to a smaller width than the initially unstrained layer. As the beam bends, the inner material experiences the same phenomenon described for the uniaxial case, favoring a more positive κ_ϕ. At equilibrium under no voltage, the negative κ_ϕ caused by the plane strain and the positive κ_ϕ caused by the beam bending nearly cancel out. As with the uniaxial case, actuation with an applied voltage tends to increase the DEA width, further increasing κ_ϕ in the positive direction. The minimal saddling in the plane strain pre-stretch case explains why its 0 voltage predictions are similar to those of the pure bending model. The saddling has the greatest effect on the effective area moment of inertia in comparison to overall width or thickness.

The theoretical predictions presented in Figs. 5 and 6 are obtained for geometries and materials constants based on the experimental DEA sample: $L_1 = L_2 = 20\,\mathrm{mm}$, $L_3 = 1.06L_1 = 21.2\,\mathrm{mm}$, $W_3 = 6.5\,\mathrm{mm}$, $b = 0.75\,\mathrm{mm}$, $H_1 = 163\,\mu\mathrm{m}$, $H_2 = 85\,\mu\mathrm{m}$, and $H_3 = 490\,\mu\mathrm{m}$. The Young's modulus, $E = 1\,\mathrm{MPa}$, was determined through tensile tests with an Instron® materials testing system (Model #4467; Instron) and is similar to values found in the literature.[20,40–43] A dielectric constant $\epsilon_r = 2.72$ is reported in the product data sheet of the materials supplier (Dow Corning, Inc.). The double integrals for computing Ω_i are performed in MATLAB R2011b and R2013a using an adaptive Simpson quadrature (*dblquad*) and Π is minimized for $\{w, \ell, \kappa_\theta, \kappa_\phi\}$ using a direct simplex search method (*fminsearch*).

V. CONCLUDING REMARKS

We have introduced an entirely soft DEA that contains no rigid or inextensible materials. It is composed of PDMS embedded with a liquid-phase GaIn alloy. After assembly, the GaIn-PDMS spontaneously deforms into a saddle-shape that changes curvature when voltage is applied to the liquid electrodes. This shape is accurately predicted with an elastic shell theory based on the principle of minimum potential energy and hyperelastic constitutive model. Since the materials undergo only moderate strains (<10%), good agreement between theory and experiment can be achieved with a NeoHookean constitutive law, which only requires a single coefficient of elasticity. In general, DEAs with large pre-stretch and bending curvature should be modeled with a more accurate nonlinear constitutive law. However, even in these cases, the proposed 4-parameter kinematic

representation for a saddle-shaped shell with negative Gaussian curvature is sufficient for predicting the shape at static equilibrium for prescribed pre-stretches and voltage. While we focused on two types of pre-stretch (so-called uniaxial and plane strain loading), the theory is sufficiently general for any biaxial loading condition on the dielectric layer prior to bonding and release.

ACKNOWLEDGMENTS

This work was supported by Young Investigator Programs from the Office of Naval Research (Program Officer: Dr. Tom McKenna; Code 34) and Air Force Office of Scientific Research (Program Officer: Dr. Les Lee; Mechanics of Multifunctional Materials and Microsystems), the National Science Foundation Graduate Research Fellowship Program, NSF Grant No. DMS 0635983 for the Center for Nonlinear Analysis at Carnegie Mellon University and FP7-PEOPLE-IAPP HOTBRICKS 2013-2017.

[1]L. R. Finkenauer and C. Majidi, SPIE Proc. **9056**, 90563I (2014).
[2]O. A. Araromi, I. Gavrilovich, J. Shintake, S. Rosset, and H. R. Shea, SPIE Proc. **9056**, 90562G (2014).
[3]R. Zhang, A. Kunz, P. Lochmatter, and G. Kovacs, 14th Symposium on Haptic Interfaces for Virtual Environment and Teleoperator Systems, part of IEEE Virtual Reality 2006 (IEEE, 2006) pp. 347–353.
[4]S. M. C. Abdulla, H. Yagubizade, and G. J. M. Krijnen, J. Micromech. Microeng. **22**, 035014 (2012).
[5]P. Lochmatter, "Development of a shell-like electroactive polymer (EAP) actuator," Ph.D. dissertation (ETH Zurich, 2007).
[6]S. Rosset, M. Niklaus, P. Dubois, H. R. Shea, and S. Member, J. Microelectromech. Syst. **18**, 1300 (2009).
[7]R. Pelrine, R. Kornbluh, and J. Joseph, Sens. Actuators, A **64**, 77 (1998).
[8]A. P. Gerratt, B. Balakrisnan, I. Penskiy, and S. Bergbreiter, Smart Mater. Struct. **23**, 055004 (2014).
[9]A. Rajamani, M. D. Grissom, C. D. Rahn, and Q. Zhang, IEEE/ASME Trans. Mechatron. **13**, 117 (2008).
[10]G. Kovacs, L. Dring, S. Michel, and G. Terrasi, Sens. Actuators, A **155**, 299 (2009).
[11]W. Lai, A. F. Bastawros, W. Hong, and S.-J. Chung, *IEEE International Conference on Robotics and Automation* (2012), p. 4968.
[12]S. Rosset and H. R. Shea, Appl. Phys. A **110**, 281 (2013).
[13]G.-K. Lau, S. C.-K. Goh, and L.-L. Shiau, Sens. Actuators, A **169**, 234 (2011).
[14]R. Palakodeti and M. Kessler, Mater. Lett. **60**, 3437 (2006).
[15]C. Keplinger, J.-Y. Sun, C. C. Foo, P. Rothemund, G. M. Whitesides, and Z. Suo, Science **341**, 984 (2013).
[16]Y. Sun, V. Kumar, I. Adesida, and J. Rogers, Adv. Mater. **18**, 2857 (2006).
[17]R. C. Chiechi, E. A. Weiss, M. D. Dickey, and G. M. Whitesides, Angew. Chem. Int. Ed. Engl. **47**, 142 (2008).
[18]Y. Liu, M. Gao, S. Mei, Y. Han, and J. Liu, Appl. Phys. Lett. **103**, 064101 (2013).
[19]H.-J. Kim, C. Son, and B. Ziaie, Appl. Phys. Lett. **92**, 011904 (2008).
[20]Y.-L. Park, C. Majidi, R. Kramer, P. Bérard, and R. J. Wood, J. Micromech. Microeng. **20**, 125029 (2010).
[21]S. Cheng and Z. Wu, Lab Chip **12**, 2782 (2012).
[22]M. D. Dickey, R. C. Chiechi, R. J. Larsen, E. A. Weiss, D. A. Weitz, and G. M. Whitesides, Adv. Funct. Mater. **18**, 1097 (2008).
[23]T. Lu, L. Finkenauer, J. Wissman, and C. Majidi, Adv. Funct. Mater. **24**, 3351 (2014).
[24]R. K. Kramer, C. Majidi, and R. J. Wood, Adv. Funct. Mater. **23**, 5292 (2013).
[25]S. H. Jeong, A. Hagman, K. Hjort, M. Jobs, J. Sundqvist, and Z. Wu, Lab Chip **12**, 4657 (2012).
[26]J. Wissman, T. Lu, and C. Majidi, IEEE Sens. **2013**, 1.
[27]R. M. McMeeking and C. M. Landis, J. Appl. Mech. **72**, 581 (2005).
[28]M. Wissler and E. Mazza, Sens. Actuators, A **138**, 384 (2007).
[29]Z. Suo, Acta Mech. Solida Sin. **23**, 549 (2010).
[30]B.-X. Xu, R. Mueller, A. Theis, M. Klassen, and D. Gross, Appl. Phys. Lett. **100**, 112903 (2012).
[31]J. Zhu, S. Cai, and Z. Suo, Int. J. Solids Struct. **47**, 3254 (2010).
[32]J. Zhu, S. Cai, and Z. Suo, Polym. Int. **59**, 378 (2010).
[33]D. De Tommasi, G. Puglisi, and G. Zurlo, J. Phys. D: Appl. Phys. **47**, 065502 (2014).
[34]G. Puglisi and G. Zurlo, J. Electrostat. **70**, 312 (2012).
[35]H. S. Park and T. D. Nguyen, Soft Matter **9**, 1031 (2013).
[36]L. R. G. Treloar, Proc. Phys. Soc. **60**, 135 (1948).
[37]M. Mooney, J. Appl. Phys. **11**, 582 (1940).
[38]R. S. Rivlin, Philos. Trans. R. Soc. London, Ser. A **241**, 379 (1948).
[39]R. Ogden, Proc. R. Soc. London Ser. A **326**, 565 (1972).
[40]Z. Wang, A. A. Volinsky, and N. D. Gallant, J. Appl. Polym. Sci. **131**, 41050 (2014).
[41]Y. M. Song, Y. Xie, V. Malyarchuk, J. Xiao, I. Jung, K.-J. Choi, Z. Liu, H. Park, C. Lu, R.-H. Kim, R. Li, K. B. Crozier, Y. Huang, and J. A. Rogers, Nature **497**, 95 (2013).
[42]D. Armani, C. Liu, and N. Aluru, in *Twelfth IEEE International Conference on Micro Electro Mechanical System* (IEEE, 1999), p. 222.
[43]A. P. Gerratt, I. Penskiy, and S. Bergbreiter, J. Micromech. Microeng. **20**, 104011 (2010).